5-2018

Inertial Particle Transport by Lagrangian Coherent Structures in Geophysical Flows

Alexa Aucoin
Montclair State University

ABSTRACT

Title of Thesis: INERTIAL PARTICLE TRANSPORT BY LAGRANGIAN COHERENT STRUCTURES IN GEOPHYSICAL FLOWS

Alexa Aucoin, Master of Science, 2018

Thesis directed by: Dr. Eric Forgoston
Department of Mathematical Sciences

Lagrangian Coherent Structures (LCS) provide a skeleton for the underlying structures in geophysical flows. It is known that LCS govern the movement of fluid particles within a flow, but it is not well understood how these same LCS influence the movement of inertial particles within a fluid flow. In this thesis, we consider two geophysical flows, the double-gyre model, and a single-layer quasi-geostrophic PDE model. In particular, we use finite-time Lyapunov exponents (FTLE) to characterize the attracting and repelling LCS for these models and show how inertial particles aggregate with respect to LCS. We numerically investigate the dynamics of inertial particles for a range of Stokes numbers and density ratios. We also examine the effects of Coriolis force on the preferential aggregation of inertial particles in the double-gyre model. Additionally, we highlight the funneling behavior of inertial particles due to the western boundary effect that arises in the quasi-geostrophic model.

MONTCLAIR STATE UNIVERSITY

INERTIAL PARTICLE TRANSPORT BY LAGRANGIAN COHERENT STRUCTURES IN GEOPHYSICAL FLOWS

by

Alexa Aucoin

A Master's Thesis Submitted to the Faculty of

Montclair State University

In Partial Fulfillment of the Requirements

For the Degree of

Master of Science with a Concentration in Pure and Applied Mathematics

May 2018

School College of Science and Mathematics

Department Mathematical Sciences

Thesis Committee:

[redacted]

Dr. Eric Forgoston
Thesis Sponsor

[redacted]

Dr. Lora Billings
Committee Member

[redacted]

Dr. Ashwin Vaidya
Committee Member

INERTIAL PARTICLE TRANSPORT BY LAGRANGIAN COHERENT STRUCTURES IN GEOPHYSICAL FLOWS

A THESIS

Submitted in partial fulfillment of the requirements

For the degree of Master of Science in Pure and Applied Mathematics

by

ALEXA AUCOIN

Montclair State University

Montclair, NJ

May 2018

Acknowledgements

AA was supported by the National Science Foundation (Award Numbers CMMI-1462884 and DMS 1418956). The content is solely the responsibility of the author and does not necessarily represent the official views of the National Science Foundation.

Contents

List of Figures

1 Introduction

Autonomous underwater vehicles (AUVs) are useful for performing a variety of sensing tasks. These tasks can range from aiding in more accurate weather prediction, predicting potential weather disasters, or tracking contaminants like oil or plastic debris in the ocean. Understanding both the fluid and inertial dynamics of complex ocean flows is crucial to using these AUVs in both energy- and time-optimal ways. Insight into the driving force behind complex fluid flows was introduced by Pierrehumbert and Yang in 1999 when they used finite-time Lyapunov exponents (FTLE) fields to describe the persisting stretching and contracting dynamics in velocity field data [1]. Shortly thereafter, George Haller rigorously connected these long-lasting high FTLE ridges to be indicators of Lagrangian coherent structures (LCS) [2]. LCS are robust structures within a flow which delineate areas of strong dynamics. As such, they can serve as the underlying skeleton for complex flows and are extremely useful in understanding fluid transport [3].

The study of fluid transport has relevant applications to a broad range of fields such as atmospheric science [4–6], engineering [7], population dynamics [8] and of course, oceanography. In particular, preferential aggregation behavior of tracer particles has been the focus of much geological fluids research. For example, particle transport of oil [9, 10], phytoplankton, and algal blooms [11, 12] have all provided motivation to study particle transport and aggregation within geophysical fluid flows. It is now known that the dynamics of fluid (passive tracer) particle transport are governed by LCS. Figure 1 provides a visual for some examples of this natural transport along known LCS. The close interaction between particle transport and LCS becomes extremely useful when theoretically informing AUV decisions during sensing tasks [13].

In practical settings, however, actual AUVs have finite size and mass and, as such, are subject to the effects of inertia. In the bottom-right image of Fig. 1, one can see the aggregation behavior of plastic debris, which, due to their finite size and mass, have fundamentally different transport behavior compared to passive tracers like oil and algae. While the relationship between fluid particle transport and coherent structures is well understood, it is not well understood how these same structures affect the transport of inertial particles. Do the same structures that govern fluid particle dynamics also govern inertial particle dynamics? If so, in what way? Are there additional structures, say inertial Lagrangian coherent structures (iLCS), that govern inertial particle dynamics? The goal of this master's thesis is to answer these questions by performing fundamental studies to determine the relationship between inertial particle transport and LCS (iLCS).

1.1 Background

In 1983, Martin Maxey and James J. Riley rigorously formalized the equations of motion for a spherical inertial particle in a non-uniform, low Reynolds number flow [18]. Their work bridged the limitations of previous works by considering all forces acting on the particle in a Stokes flow regime. In addition to the added mass term that many of their predecessors used, Maxey and Riley accounted for drag, lift and shear effects. Their careful work resulted in the self-named Maxey-Riley equation which describes the motion of a rigid sphere within a fluid flow. The Maxey-Riley equation for $\dot{v}$, where v is the velocity of a spherical inertial particle in an undisturbed flow, is given in dimensional form by

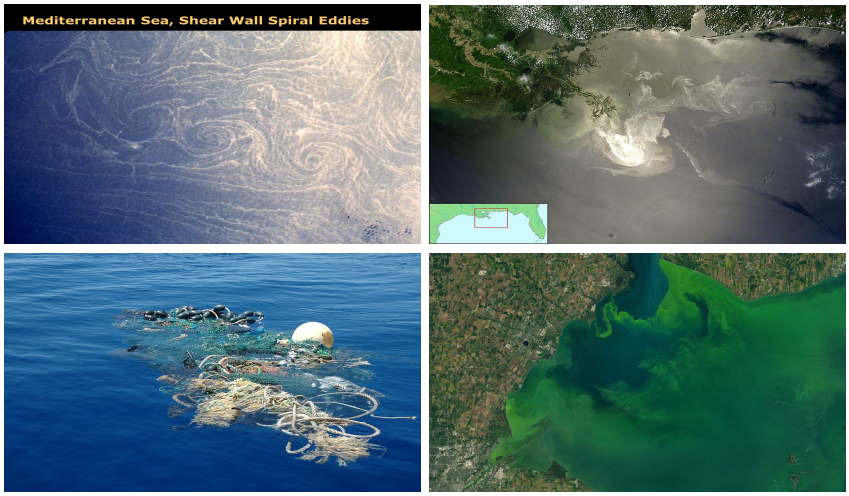

Figure 1: Instances of coherent structures in nature. Clockswise from the top-left: Streamlines of Mediterranean eddies highlight expected paths of passive tracer particles [14]; Deepwater Horizon oil spill along the Gulf of Mexico [15]; Algal bloom dispersing along known LCS in Lake Eerie [16]; Plastic debris collecting in the Pacific ocean [17].

$$\begin{aligned} m_p\dot{v} = m_f\frac{D}{Dt}u(r(t),t) - \frac{1}{2}m_f\frac{d}{dt}[v - u(r(t),t) - \frac{1}{10}a^2\nabla^2 u(r(t),t)] \\ -6\pi a\mu X(t) + (m_p - m_f)g - 6\pi a\mu\int_0^1 d\tau \frac{\frac{dX(\tau)}{d\tau}}{\sqrt{\pi\nu(v(t-\tau))}} \end{aligned} \tag{1}$$

where

$$X(t) = v(t) - u(r(t),t) - \frac{1}{6}a^2\nabla^2 u.$$

This is a mass formulation with m_p the mass of the inertial particle and m_f the mass of the fluid displaced by the particle. This form is consistent with the more popularly used density formulation used in [19] and many other works. The velocity of the fluid is given by $u(r(t),t)$ which describes the fluid velocity at position $r(t)$ and time t. One also must describe the viscosity of the carrier fluid, μ, the radius of the inertial particle, a, and the acceleration due to gravity, g. It is also important to distinguish the two derivatives present in the equation: $\frac{d}{dt}$ represents the usual total derivative with respect to time, where as $\dfrac{D}{Dt}$ represents the material derivative so that

$$\frac{Du}{Dt} = \frac{\partial u}{\partial t} + u\nabla u.$$

Term by term, the right-hand side of Eq. 1 describes the undisturbed fluid force on the particle, added mass, Stokes' drag and buoyancy effects. The Basset history term and the Faxèn correction term are given by the integral term and $a^2\nabla u$ respectively. Analysis of the Maxey-Riley equations can be found in Chapter 9 of Ref. [20] as well as a detailed review in Ref. [21].

In practice, the Faxèn correction and Basset history terms are often neglected for simplicity.

By neglecting the Faxèn term, we are assuming the size of the particles, a, is sufficiently small. Neglecting the Basset history term requires making some assumptions on the time scales of the problem which are appropriate for this work. In essence, we assume the characteristic time for a particle to return to a specific region is much longer in comparison to the time scale of our problem. Insight on the effects of including the history term for inertial particles of varying density can be found in Ref. [22]. For the purposes of this work, we will also neglect the buoyancy term and the effects of gravity. Using the fluid flow's velocity scale U and length scale L, we obtain the dimensionless form of Eq. 1

$$\ddot{r}(t) = \frac{1}{St}(u(r(t),t) - \dot{r}(t)) + \frac{3}{2}R\frac{d}{dt}(u(r(t),t)), \tag{2}$$

where the Stokes number St is in essence a characteristic relaxation time of the particle to the underlying fluid flow. The inertial particles will follow the flow more closely in low Stokes number flows versus high Stokes number flows. The density ratio parameter, R, compares the density of the inertial particle to the density of the carrier fluid. The dimensionless form of these terms are

$$St = \frac{(m_p + \frac{1}{2}m_f)U}{6\pi a\mu L}$$

and

$$R = \frac{m_f}{m_p + \frac{1}{2}m_f}.$$

In the case of neutrally buoyant particles, the density of the carrier fluid and the density of the inertial particle are exactly equal making $R = 2/3$. When $R > \frac{2}{3}$, the particle is lighter than the carrier fluid, and when $R < \frac{2}{3}$ the particle is heavier than the carrier fluid. We refer to the light and heavy particles as bubbles and aerosols respectively throughout the remainder of this thesis.

Using the simplified Maxey-Riley equation given by Eq. 2, Sudharsan et al. [23] studied the aggregation behavior of inertial particles in a simple double-gyre model. For inertial particles of varied densities (heavy, light, and neutrally buoyant with respect to fluid particles), they showed that fluid LCS influence the preferential aggregation behavior of inertial particles. They concluded that heavy particles prefer to aggregate along LCS ridges, while light particles exhibit preferential aggregation in the center of the gyres, suggesting bubbles are repelled by those same structures. In the case of neutrally buoyant particles, which have the same density as the carrier fluid particles, inertial particles behave as expected, following the same trajectories as passive tracers. This study also took a cursory look at how the inertial particle behavior changed with a slight variation of the Stokes numbers.

1.2 Novelty of this work

This thesis work differs from previous work in its exploration of inertial particle aggregation for varied Stokes numbers and particle densities for the double-gyre model, as well as investigating a more realistic PDE fluid model. Additionally, in order to more closely mimic oceanic flows, we consider these same models with inertial particles subjected to the Coriolis force and provide the same comprehensive study with respect to particle densities and Stokes numbers. These studies offer new insight about the additional influences of inertial particle transport. Lastly, we extend our exploration to experimental data, which was obtained in our fluids laboratory using a flow tank capable of generating a variety of ocean-like flows and Particle Imaging Velocimitry (PIV).

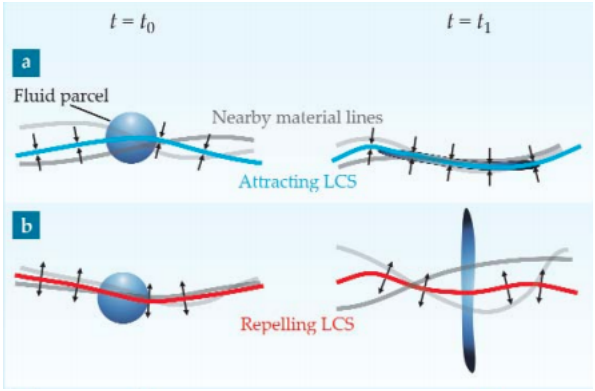

Figure 2: Deformation of a single fluid particle along attracting (blue) and repelling (red) material lines. The deformation occurs over a time interval $I = [t_0, t_1]$. We see the fluid parcel stretch along attracting LCS, while repelling LCS cause the particle to stretch in the normal direction away from the material line. The figure was obtained from Ref. [3].

2 Theory and Methodology

2.1 Lagrangian coherent structures

Oceanic flows are time-dependent and often aperiodic. With a sensitivity to initial conditions, these characteristics make flow dynamics uncertain and difficult to predict. Lagrangian coherent structures (LCS), however, are robust features of these otherwise unstable flows. LCS most dominantly influence nearby trajectories and are responsible for creating the coherent patterns we see in nature. Specifically, LCS discern the most attracting, repelling and shearing behavior of material lines over time and, as such, become a useful tool for describing complex flow dynamics. To delineate these highly dynamic regions, we measure the deformation of fluid parcels along material lines. The theory for computing LCS is given in detail in Ref. [24]. Here, we provide the reader with a visual example of LCS dynamics in Fig. 2 which highlights the difference in fluid parcel deformation along attracting and repelling LCS. Figure 2(a) shows a spherical fluid particle initiated on an attracting material line. After some finite time t_1, the particle stretches along the material line. This deformation behavior indicates an attracting LCS. In contrast, Fig. 2(b) depicts the deformation of a fluid parcel initiated on a repelling material line. In this case, the particle is repelled and stretched away from the material line. Coherent structures are made up of these material lines associated with the highest deformation dynamics. From a dynamical systems perspective, LCS play similar roles to the stable and unstable manifolds in a nonlinear system. For complex, time-dependent flows, LCS are crucial to understanding flow dynamics where stable and unstable manifolds are not necessarily defined [25].

Many different methods have been used to determine the location of LCS with varied success. Due to the substantial numerics necessary for this work, we utilize finite-time Lyapunov exponents (FTLE) which are relatively simple to compute and serve as a good proxy for determining LCS for the fluid flows we consider.

2.2 Finite-time Lyapunov exponents

Finite-time Lyapunov exponents are commonly used to compute coherent structures within fluid flows and have been justified as a tool to determine LCS [26–28]. Consider any arbitrary two-dimensional velocity field defined on a domain D given by

$$\dot{x} = u(x,t) \text{ for any } x \in D \subset \mathbb{R}^2 \tag{3}$$

and defined on a time interval $I = [t_0, t_0+T]$. Then the trajectory of a particle initiated at starting position x_0 and time t_0, written as $x(t;t_0,x_0)$, will be a solution to the dynamical system

$$\begin{cases} \dot{x}(t;t_0,x_0) = u(x(t;,t_0,x_0)), \\ x(t_0;t_0,x_0) = x_0. \end{cases} \tag{4}$$

Fixing the initial time, t_0, and a desired finite time, T, the solution of Eq. 4 acts like a flow map which maps a particle starting at time t_0 from its initial position x_0 to its corresponding position at the final time t_0+T. We define the flow map

$$\phi_{t_0}^{t_0+T} : D \to D : x_0 \to \phi_{t_0}^{t_0+T}(x_0) = x(t;t_0,x_0) \tag{5}$$

to describe the advection of a grid of uniformly spaced particles over the entire domain D [29]. In essence, the finite-time Lyapunov exponent measures the separation between trajectories of a pair of initially close particles over the chosen finite time T. The FTLE is given by

$$\sigma(x,t_0+T,T) = \frac{1}{|T|} ln(\sqrt{\lambda_{max}(\Delta)}, \tag{6}$$

where

$$\Delta(x,t_0+T,T) = \left(\frac{d\phi_{t_0}^{t_0+T}(x(t))}{dx(t)}\right)^* \left(\frac{d\phi_{t_0}^{t_0+T}(x(t))}{dx(t)}\right)$$

is the right Cauchy-Green deformation tensor, $*$ denotes the adjoint, and $\lambda_{max}(\Delta)$ is the associated maximum eigenvalue of Δ.

Computing FTLE values at every point in the domain results in the FTLE field of the flow for a chosen finite time. Areas in which nearby particles separate dramatically over time will have high FTLE values, while regions where nearby particles stay close together will yield low FTLE values. In 2001, it was shown by Haller that ridges of high FTLE values are indeed indicators of LCS. High FTLE ridges correspond to repelling LCS in forward time and attracting coherent structures in backwards time. For more detailed theory behind this connection, interested readers are referred to Ref. [2].

2.3 Modified Maxey-Riley equation

In order to obtain the FTLE fields for fluid or inertial particles, we start with a uniform grid of particles at an initial time t_0 and numerically integrate out to the finite-time T. For fluid particles, this process is relatively simple. We can use the equations from existing fluid models to obtain velocity field data and integrate over a desired finite-time. For this work, we use the well-studied double-gyre ODE model, and a quasi-geostrophic PDE model derived from first principles. These

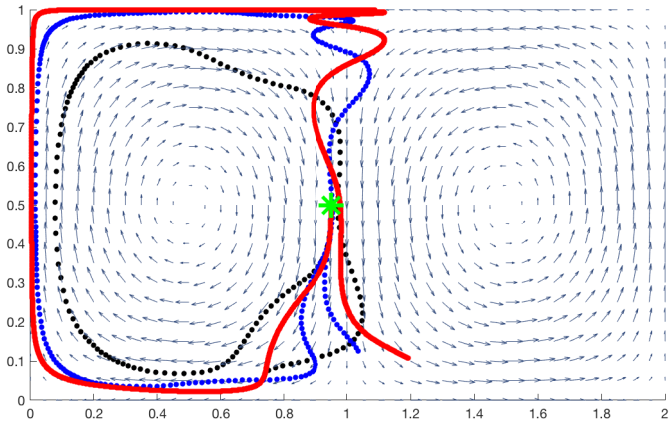

Figure 3: The path of a passive tracer (black), an inertial aerosol particle (red), and an inertial aerosol particle under the influence of Coriolis force (blue), are shown for the same initial position $(x, y) = (0.95, 0.8)$. The three paths diverge from another quickly, highlighting their different dynamic behaviors.

models are discussed further in Section 3.

Integrating the inertial particles over time is more involved. We must numerically integrate Eq. 2 for both the position and velocity of the inertial particles at each time step. In an effort to model inertial particle dynamics more realistically, we also modify the Maxey-Riley equation to account for the effects of the earth's rotation. Coriolis force effects can be captured by adding an additional term to Eq. 2 so that one obtains

$$\ddot{r}(t) = \frac{1}{St}(u(r(t),t) - \dot{r}(t)) + \frac{3}{2}R\frac{d}{dt}(u(r(t),t)) \underline{-2\Omega \times \dot{r}(t)}, \tag{7}$$

where the underlined term is the Coriolis force term. In this work, results which explicitly mention the Coriolis force acting on inertial particles were computed using Eq. 7. Otherwise, results were computed using the usual simplified Maxey-Riley equation given by Eq. 2.

We employ a fourth-order Runge-Kutta method to numerically integrate both fluid and inertial particles through the system. Since we are measuring the exponential contraction/stretching of particle trajectories, a sufficiently small spatial grid size and temporal step size is needed to obtain accurate results. In most instances, we employ a spatial step size $dx = dy \leq 0.05$ and a temporal step size $dt \leq 0.01$.

Figure 3 highlights the trajectories of a passive tracer particle and inertial aerosol particles with and without the presence of Coriolis force. These paths, initiated at the same position, diverge very quickly from one another. This figure serves to highlight the importance of this work and its consideration for physically relevant forces. It is clear that passive tracers and inertial particles behave in fundamentally different ways and the Coriolis force definitely impacts inertial particle transport. In order to optimally utilize AUVs in the ocean, we need to understand the effects of all of the forces at play.

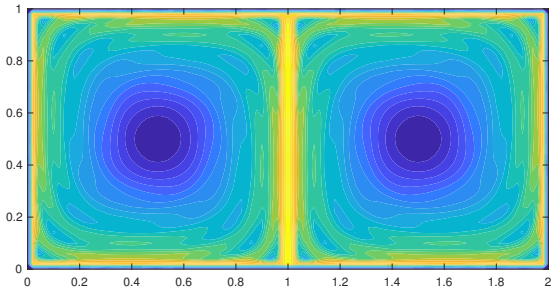

Figure 4: Backwards time FTLE of the time-independent double-gyre model highlights attracting LCS in forward time.

2.3.1 Extending the Maxey-Riley equations

The Maxey-Riley equation of motion was developed by considering small spherical particles in low Reynolds number flows. The work of this thesis is motivated by the use of practical AUVs, which are not spherical, in oceanic flows, which possess high Reynolds number regimes. A natural question is how we can justify that our work is in fact applicable and influential to the application of interest.

To begin, the equation of motion of an object in a flow originated with the Lagrangian method of Kelvin and Kirchhoff, who considered rigid spheres immersed in unbounded, high Reynolds number (inviscid) fluids, and identified the now well-known added mass effect. Basset and Boussinesq later took a low Reynolds number approach, finding, in addition to added mass, a history effect, now called the Basset force [30]. While this history effect depends on viscosity, it is not restricted to low Reynolds numbers. Developments of this model, in particular by Oseen (the BBO model), resulted in other corrections that were also not restricted to a low Reynolds number limit. While a purely inviscid approach (based on the Lagally theorem) is pursued in some problems, more work has been focused on reconciling the low and high Reynolds number applications of the basic models and quantifying the validity of their individual forces in those limits. Recently, the high Reynolds number use of BBO and Maxey-Riley (MR) type models was reviewed, citing their successes in applications when individual forces are parameterized. It is therefore not unusual that MR-type models, which extend BBO models to account for flow non-uniformities, have been applied to a wide range of conditions, including Reynolds numbers up to 16,000.

Apart from Reynolds number, a restriction of the above models is that only spherical objects are considered, excluding their application to the motion of realistically shaped objects. Yet it is well-known from the design of vehicles and the study of biolocomotion, that shape plays a critical role in the forces of flow on an object. In most cases, the role of shape in modifying the forces exerted on an object in a flow is directly captured by the forces (drag, added mass, lift) described in the BBO or MR models or their high Reynolds number extensions.

3 Fluid Models

3.1 Double-gyre flow model

We begin our exploration with the double-gyre (DG) model. This model is a natural starting point for many projects due to its simplicity. It is a well-studied fluid model consisting of two counter-rotating vortices. The velocity field for the double-gyre model is given by

$$\dot{x} = -\pi A \sin(\pi f(x,t)) \cos(\pi y) - \alpha x, \tag{8a}$$

$$\dot{y} = \pi A \cos(\pi f(x,t)) \sin(\pi y) \frac{df}{dx} - \alpha y, \tag{8b}$$

$$f(x,t) = \epsilon \sin(\omega t + \psi) x^2 + (1 - 2\epsilon \sin(\omega t + \psi) x), \tag{8c}$$

where $\frac{\omega}{2\pi}$ is the frequency of oscillations, A is approximately the amplitude of the velocity vectors, ϵ is the frequency of sloshing of the separatrix, ψ is the phase, and α is the dissipation. For our purposes, we let $\psi = 0$ and $\alpha = 0$ and consider no dissipation. When $\epsilon = 0$ there is no left and right motion of the separatrix, so the flow becomes time-independent. We study both time-independent and time-dependent flows, the latter being of much more interest in applications to oceanic flows.

3.1.1 Double-gyre FTLE field

The simplest version of the double-gyre model is the time-independent case, when $\epsilon = 0$. There is no periodic left-right sloshing of the gyres, resulting in a true separatrix between the two gyres. In a $[0, 2]$x$[0, 1]$ domain, Eq. 8 gives rise to two gyres centered at $(0.5, 0.5)$ and $(1.5, 0.5)$. In the time-independent case, there is a true separatrix, a heteroclinic trajectory connecting a saddle node at $(1, 0)$ to a saddle node at $(1, 1)$. From a dynamical systems perspective, it is easy to understand that a pair of particles initiated on either side of this separatrix will be advected away from one another over time, suggesting there will be high FTLE values along the separatrix. Since there is no

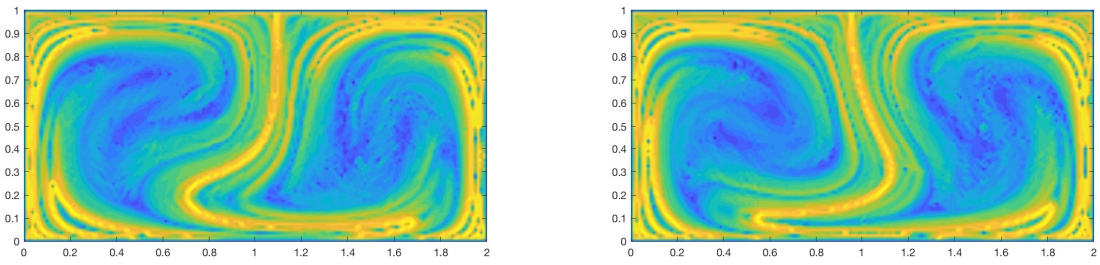

Figure 5: Backwards time FTLE of the double-gyre model with periodic sloshing $\omega = \frac{6\pi}{10}$ and finite time $T = 15$. The left figure is captured at $t = 15$ and the right figure at $t = 22.5$. The thin bands of high FTLE values computed in backwards time highlight the attracting LCS. Other parameters include $\epsilon = 0.25$ and $A = 0.1$

change in the underlying flow over time, the FTLE field remains constant in time. Computing the FTLE field for the time-independent double-gyre model indeed yields high FTLE values along the separatrix (Fig. 4). In backwards time, this high FTLE ridge represents an attracting LCS. To model a more realistic oceanic flows, we consider the time-dependent double-gyre, $\epsilon \neq 0$, where the left-right sloshing emulates wind-forcing. In this work, we study the double-gyre model for modest sloshing frequency $\omega = \frac{6\pi}{10}$. The sloshing gives rise to a pair of counter-rotating vortices which periodically oscillate back and forth in the x direction. In this case, the FTLE field will changes in time, as do the LCS that govern passive tracer transport. In fact, the coherent structures obtained in this case periodically evolve with the same oscillation frequency. Figure 5 shows two snap shots in time of these evolving FTLE fields. The periodic sloshing results in a deformation of the straight line FTLE ridge seen in the time-independent case. We also see that sloshing gives rise to thicker regions of strong attraction dynamics along the boundary of the gyres.

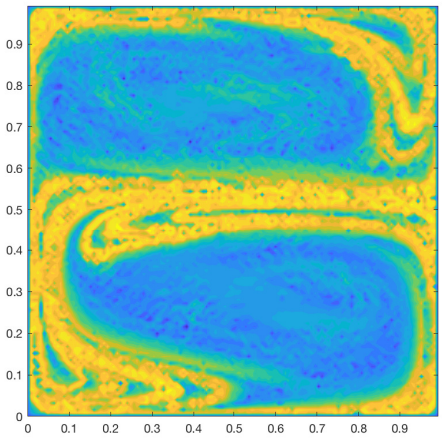

Figure 6: FTLE field for the QG model with no western boundary effects ($\beta = 0$). Sloshing of the gyres in the y-direction occurs at a rapid frequency of $\omega = 9$

3.2 Quasi-geostrophic model

The quasi-geostrophic (QG) model describes a wind-driven gyre flow based on first principles. The model considers Coriolis force, lateral stress curl and the curl of stress by winds on the sea-surface to define the streamlines of a multi-gyre flow [31]. In our work, we consider a single-layer, quasi-geostrophic double-gyre. We are interested in the model because a double-gyre flow with a realistic western boundary current is a solution that falls out naturally from the model. We define the single-layer quasi-geostrophic model over a basin $\Omega : [0, 1] \times [0, 1]$. The boundary conditions are no normal flow and free slip parallel to each of the boundary walls. The model is governed by ψ, the nondimensionalized stream function given by

$$\frac{\partial \nabla^2 \psi}{\partial t} + \epsilon J(\psi, \nabla^2 \psi) + \frac{\partial \psi}{\partial x} = \mu \nabla^2 \psi + W \tag{9}$$

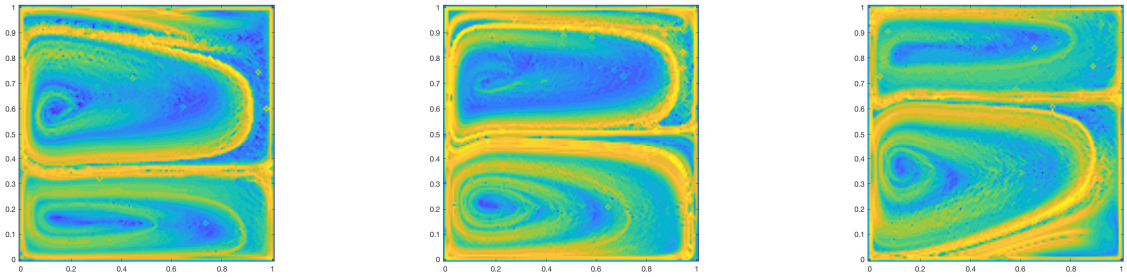

Figure 7: FTLE fields for the QG model with low frequency sloshing, $\omega = 1$, at $t = 0.1$, $t = 1.25$, and $t = 2.5$. Low frequency sloshing helps to preserve the gyre structure which remain well-defined by surrounding high FTLE ridges.

where J is the Jacobian operator

$$J(f, g) : \frac{\partial f}{\partial x}\frac{\partial g}{\partial y} - \frac{\partial g}{\partial x}\frac{\partial f}{\partial y}.$$

The parameters $\mu = \dfrac{-R}{\beta L}$ and $\epsilon = \dfrac{U}{\beta L^2}$ are dimensionless parameters which characterize the behavior of the system. The non-dimensionalized form given in Eq. 9 is specific to the case when β, the rotation parameter, is non-zero. The other parameters R L and U are the bottom friction and basin's characteristic length and velocity scales respectively. The wind-stress curl, W provides the forcing of the model and gives rise to a double-gyre circulation with periodic sloshing. The forcing W is described by

$$W = -sin(2\pi y) + 2\alpha\pi sin(\omega t) \tag{10}$$

where α is the amplitude and ω is the frequency of the periodic sloshing [32, 33].

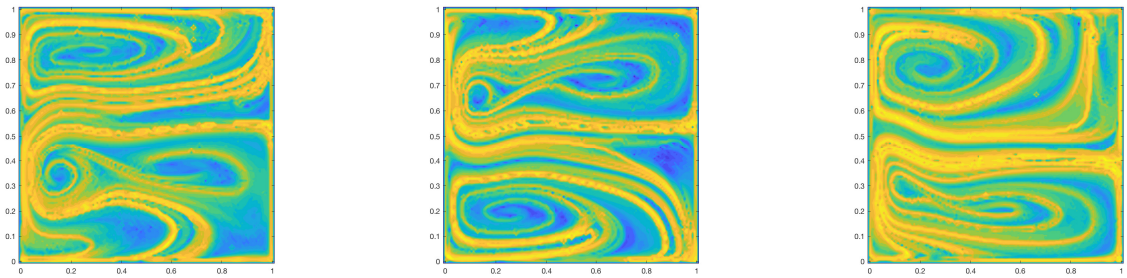

Figure 8: FTLE fields for the QG model exhibiting modest frequency sloshing, $\omega = 3$, at $t = 0.1$, $t = 1.25$, and $t = 2.5$. Modest sloshing allows for more mixing between the north and south gyres. There are more bands of high FTLE ridges when compared with the low frequency sloshing case.

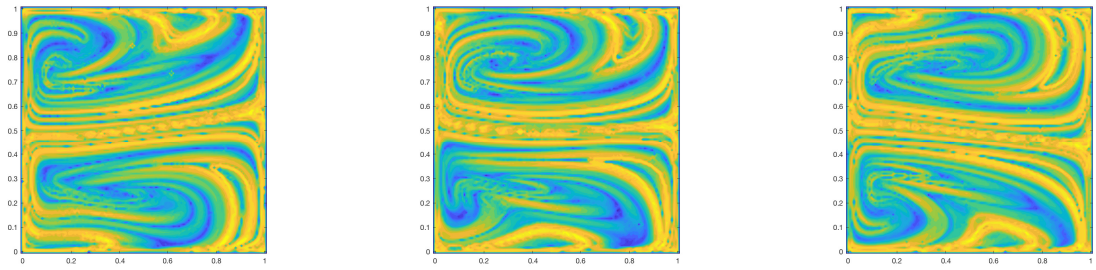

Figure 9: FTLE fields for the QG model exhibiting high frequency sloshing, $\omega = 9$, at $t = 0.1$, $t = 1.25$, and $t = 2.5$. Quick periodic sloshing results in more complicated coherent structures. We see thicker FTLE bands between the gyres and much more ribboning of high FTLE bands within the gyres.

3.2.1 Quasi-geostrophic FTLE fields

Compared to the double-gyre model, the quasi-geostrophic model captures the dynamics of real world ocean flows more realistically. One consequence of this realistic PDE model is the presence of a thin, western boundary layer. which is a phenomenon we see evidence of in real-world flows. Although it is more realistic, it adds a layer of complexity to the model. Without the western wind phenomena, the QG model behaves a lot like a vertical double-gyre model. Figure 6 shows the FTLE field for the QG model when there is no western boundary effect. Physically, the lack of a western boundary effect is present at certain longitudes on the earth's surface. In 1939, Rossby concluded that the most dynamic effects of earth's sphericity can be locally captured by the variation of Coriolis force with latitude. In other words, the rotation of the earth will have varying degrees of effect depending predominantly on where the flow is located on the globe. This position is captured by an intrinsic parameter which we refer to as the β-plane [34, 35]. The flows in which there is no western boundary effect are those flows which occur on the $\beta = 0$ plane. When $\beta \neq 0$, the western boundary effect causes significant change to the FTLE fields of the QG model. For the same sloshing frequency as the $\beta = 0$ case, the FTLE field becomes more complex, as shown in Fig. 8. We see the presence of more, thin bands of significant FTLE values as compared to just one thick FTLE band surrounding the gyres.

The FTLE fields become further complicated as we vary the frequency of the sloshing motion in the y-direction. Figures 7, 8 and 9 show the FTLE fields of the QG model for varied sloshing frequency ω at time instances $t = 0.1$, $t = 1.25$, and $t = 2.5$. As ω increases, there is much more mixing behavior present, resulting in more complicated FTLE fields. These FTLE fields suggest the intuitive notion that more frequent sloshing promotes mixing behavior, thus allowing particles to stretch away from one another and yield more complex FTLE fields.

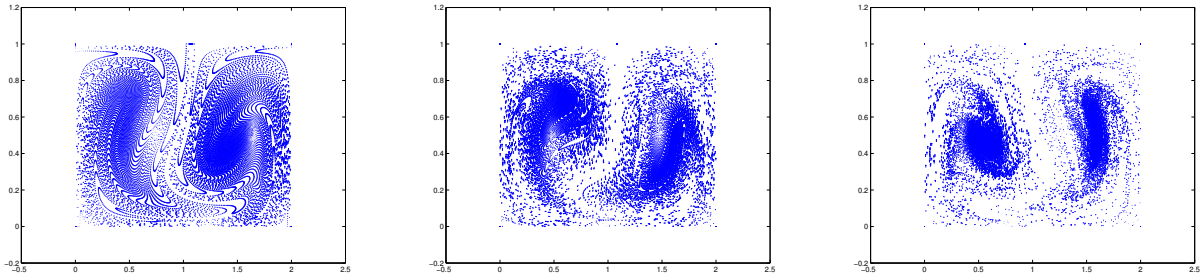

Figure 10: Preferential aggregation for bubbles ($R = 0$) at instances $t = 7.5$, $t = 15$, and $t = 22.5$. An 81×161 uniform grid of inertial particles was seeded at time $t = 0$ and advected using the double-gyre model with no Coriolis force. We see bubbles aggregating toward the center of the double-gyres. This behavior suggests bubbles are being repelled by the coherent structures shown in Fig. 5. Other parameters include: $\omega = \frac{6\pi}{10}, \epsilon = 0.25, A = 0.1$.

4 Inertial Particles in a Double-Gyre Flow

4.1 Introduction

Preferential aggregation of inertial particles for a few density ratios, R, and a few choices of Stokes number, St, was studied in Ref. [23]. For the simpler double-gyre model with no added Coriolis force, Sudharsan et. al. determined that light inertial particles with $R > \frac{2}{3}$ will aggregate towards the centers of the gyres while heavy particles $R < \frac{2}{3}$ preferentially aggregate toward the ridges of the corresponding fluid FTLE. Figures 10 and 11 illustrate their results for preferential concentration behavior for density ratios $R = 0$ and 1. When $R = \frac{2}{3}$, the inertial particles have the same density as the carrier fluid and will mimic the trajectories of passive fluid particles in the same base flow.

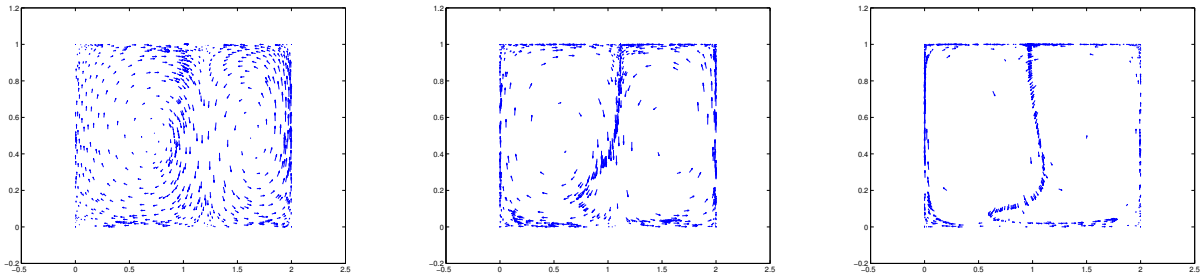

Figure 11: Preferential aggregation for aerosols ($R = 1$) at instances $t = 7.5$, $t = 15$, and $t = 22.5$. A 21×41 uniform grid of inertial particles was seeded at time $t = 0$ and advected using the double-gyre model with no Coriolis force. We see aerosols aggregating along the high FTLE ridges shown in Fig. 5. Aerosols are attracted to these coherent structures. Other parameters include: $\omega = \frac{6\pi}{10}, \epsilon = 0.25, A = 0.1$

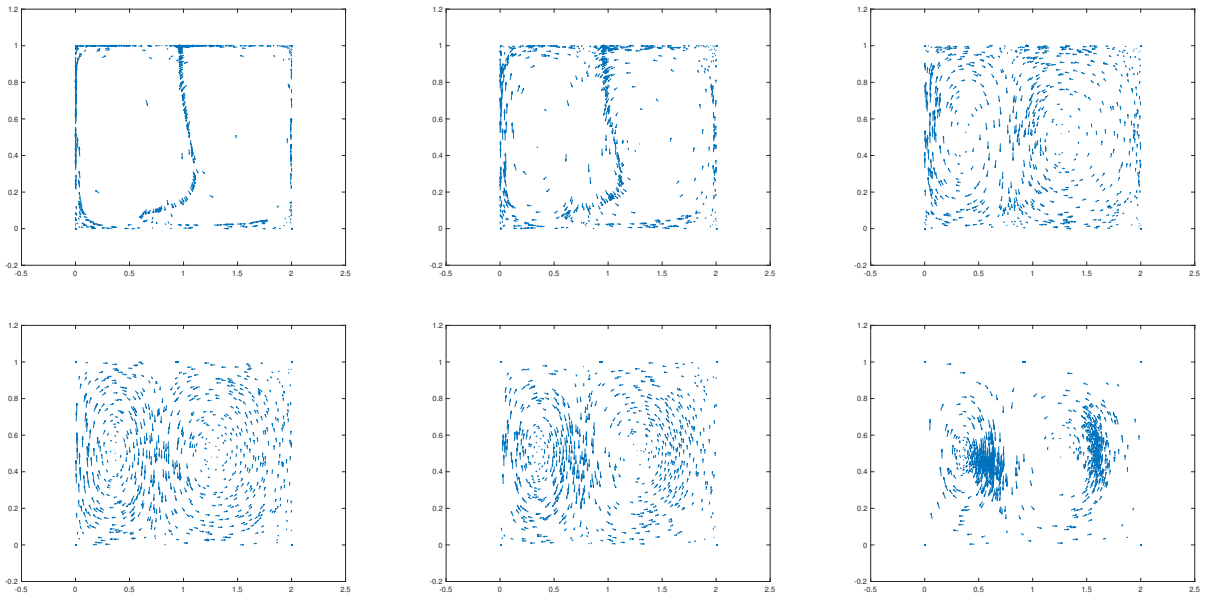

Figure 12: Preferential aggregation for a range of particle densities, $R = \left\{0, \frac{1}{4}, \frac{1}{2}, \frac{2}{3}, \frac{3}{4}, 1\right\}$. A 21×41 uniform grid of inertial particles was seeded at time $t = 0$ and advected using the double-gyre model without Coriolis force. For $R < 2/3$, particles aggregate toward the center of the double-gyres, whereas for $R > 2/3$, particles aggregate along the coherent structures shown in Fig. 5. Other parameters include: $\omega = \frac{6\pi}{10}, \epsilon = 0.25, A = 0.1$

4.2 Effect of density ratio R

We further investigate the limiting behavior of the density ratio R by testing more intermittent values between 0 and 1. Recall that Ref. [23], studied only the very heavy aerosols, $R = 1$, and very light bubbles, $R = 0$. Fig. 12 illustrates the preferential clustering of inertial particles in the same underlying flow for varied R. Moving left to right, and top to bottom, we compare the aggregation of inertial particles with density ratios $R = \left\{0, \frac{1}{4}, \frac{1}{2}, \frac{2}{3}, \frac{3}{4}, 1\right\}$ at the same time instance, $t = 15$. As expected, for intermittent density ratios, the preferential aggregation behavior is not as strong. As $R \to \frac{2}{3}$ from either direction, the aggregation of inertial particle weakens and we see the particles following the underlying flow. Inertial particles just slightly heavier than the carrier fluid $R = \frac{1}{2}$ begin to exhibit the preferential aggregation behavior, collecting along the outsides of the gyres and becoming more sparse towards the center. Particles just slightly lighter than the carrier fluid, with $R = \frac{3}{4}$, show the start of some collection behavior inside the gyres and away from the center material line. This bolsters the claim that the density of inertial particles plays an important role in their interaction with LCS. Particles with very different densities to that of the carrier fluid will exhibit much more dynamic behavior.

4.3 Effect of Stokes number

Sudharsan et. al. also highlighted the role of Stokes number St in inertial particle dynamics. Recall the Stokes number St describes the characteristic relaxation time of the inertial particle

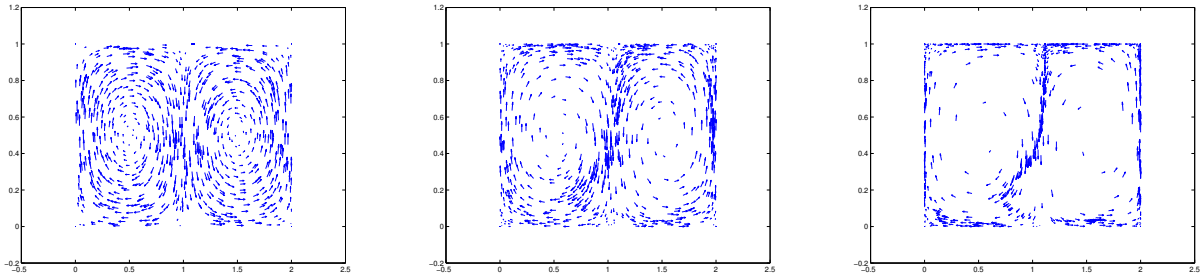

Figure 13: Preferential aggregation for aerosols ($R = 0$) at $t = 15$ for varied Stokes number, $St = \{0.01, 0.1, 0.2\}$. For low Stokes numbers, inertial particles take longer to react to the forces of the fluid flow, and as such, take longer to exhibit their preferential behavior. For high Stokes number, preferential concentration behavior is exhibited more quickly. Other parameters include: $\omega = \frac{6\pi}{10}, \epsilon = 0.25, A = 0.1$

to the underlying fluid flow. As $St \to 0$, inertial particles adhere quickly to the dynamics of the underlying flow. Note that due to the nature of Eq. 2, as $St \to 0$, the numerical methods require much smaller time steps to avoid numerical instabilities. Sufficient temporal time steps must be utilized in order to achieve sufficient accuracy.

For limited St range, Sudharsan et. al. showed that low St flows allow particles to aggregate more aggressively towards their preferred regions. Heavy particles attract along a thin high FTLE valued ridge more rapidly in low Stokes flows. Light particles advect into the gyre centers aggressively. Conversely, in higher St regimes, preferential aggregation of inertial particles is slowed. Aerosols take longer to advect onto high FTLE ridges and light particles exhibit slow aggregation toward the gyre centers. Figure 13 highlights the aggregation behavior of aerosol particles for varied Stokes flows.

4.4 Effect of Coriolis force

As discussed in Section 2.3, we added the Coriolis force to the Maxey-Riley equation in an effort to model more realistic geophysical phenomenon. The double-gyre model is well-studied and as such provides a nice benchmark for qualitatively understanding the effects of Coriolis force. We perform the same density ratio study and observe the differences in aggregation behavior in the presence of Coriolis force.

Recall that neutrally buoyant particles, $R = 2/3$, behave like passive tracer particles without the presence of Coriolis force. With Coriolis force, neutrally buoyant particles exhibit more interesting aggregation behavior. With density ratio $R = \frac{2}{3}$, particles under the influence of Coriolis force show preferential aggregation behavior towards the center of the double-gyres. Surprisingly, this behavior is more similar to the behavior of light inertial particles with no Coriolis force present. In the presence of Coriolis force, light particles again advect toward the center of the gyres. The Coriolis force seems to act as a catalyst for this preferential aggregation. Under the influence of the Coriolis force, bubbles aggregate in the center of the gyres faster and in a tighter cluster. The change in behavior for inertial particles with $R \leq \frac{2}{3}$ in the presence of Coriolis force suggests that the force makes the attractors in the center of the gyres stronger. With the Coriolis force pulling

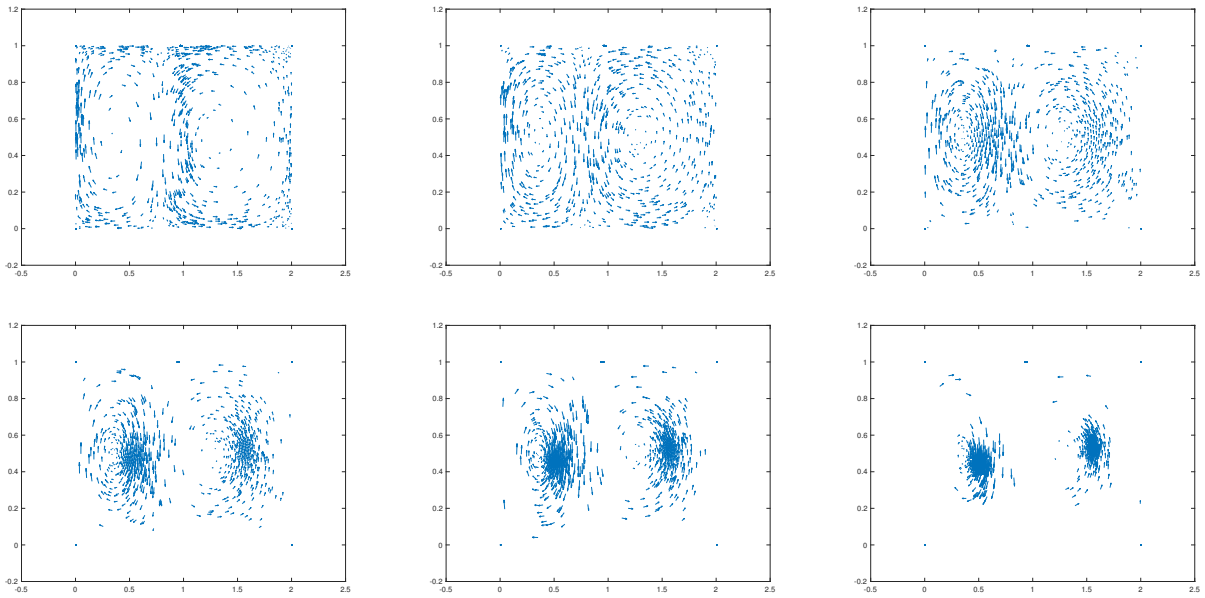

Figure 14: Preferential aggregation for a range of particle densities (moving left to right, top to bottom) $R = \left\{0, \frac{1}{4}, \frac{1}{2}, \frac{2}{3}, \frac{3}{4}, 1\right\}$. A 21×41 uniform grid of inertial particles was seeded at time $t = 0$ and advected using the double-gyre model with added Coriolis force. Other parameters include: $\omega = \frac{6\pi}{10}, \epsilon = 0.25, A = 0.1$

the inertial particles toward the gyre centers, we see faster clustering of bubbles and some new aggregation behavior of neutrally buoyant particles. By making the attraction of the center gyres stronger, the Coriolis force slows down the preferential aggregation behavior of aerosols, which typically tend to run away from the gyre centers.

The aggregation behavior of aerosols under the influence of the Coriolis force also corroborates this idea. For inertial particles with $R < \frac{2}{3}$, particles aggregate along the coherent structures shown in Fig. 11. Under the influence of the Coriolis force, we see the preferential behavior of these aerosols is slowed. The heavy particles still exhibit clustering along the center high FTLE ridge, however, this cluster appears wider, less defined, and occurs over a longer period of time.

The visualizations for these new aggregation behavior is illustrated by Fig. 14. The change in aggregation behavior suggests the presence of Coriolis force strengthens the attraction to the center of the gyres and slows attraction along the high FTLE ridge. In other words, in the double-gyre system, the Coriolis force strengthens repelling LCS while weakening attracting LCS.

5 Inertial Particles in a Quasi-Geostrophic Flow

While the double-gyre model is an appropriate starting point for this work, it does not account for many of the forces present in real-world oceanic flows. The quasi-geostrophic model, a PDE model derived from first principles, captures many of these forces and is a much more realistic model. We test our conclusions on the preferential aggregation behavior for both heavy and light particles,

and also explore the effects of Coriolis force acting on inertial particles in this more realistic model.

5.1 Effect of Western boundary current

The most interesting inertial particle behavior for the quasi-geostrophic model comes from the seemingly boring neutrally buoyant case. We expect that particles with the same density as the carrier fluid will behave similarly to fluid tracer particles; following the flow and exhibiting no preferential aggregation behavior. However, an interesting phenomenon occurs in the case of neutrally buoyant particles in the quasi-geostrophic flow.

Figure 15 compares the aggregation behavior of neutrally buoyant particles with and without the presence of the western boundary layer. When $\beta = 0$, there is no western boundary effect, and we see the expected behavior of neutrally buoyant particles. There is no preferential clustering and the particles tend the follow the flow. However, subject to western boundary effects, neutrally buoyant particles do not adhere to the underlying flow. A progression of the velocity field over time reveals some funneling behavior along a thin material line which we suspect to be the evolving LCS.

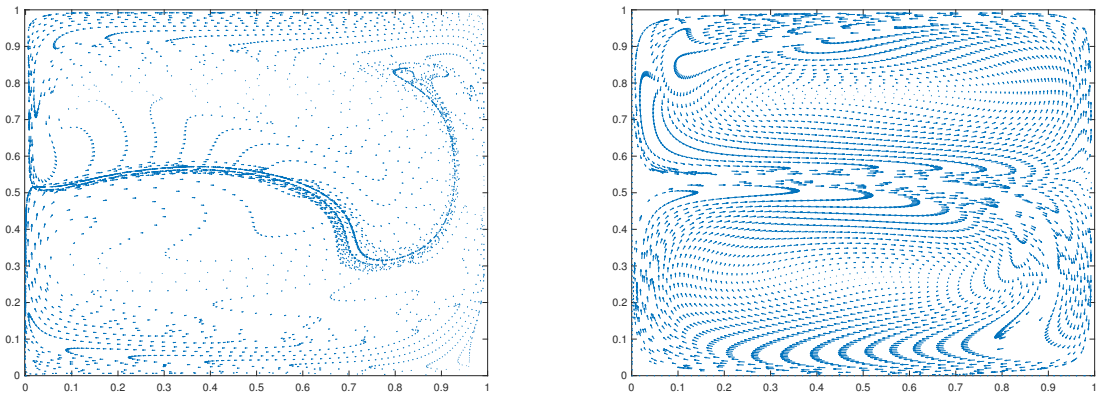

Figure 15: Aggregation behavior of neutrally buoyant particles with western boundary effects on the left and no western boundary effects ($\beta = 0$) on the right. A 64 x 64 uniform grid of inertial particles was initiated after a 5 second spin-up time. Sloshing of the gyres in the y-direction occurs at a rapid frequency $\omega = 9$.

5.2 Effect of density ratio R

We have already shown that aerosols aggregate along fluid LCS while bubbles are repelled from the same LCS in the double-gyre model. This behavior holds true in the QG model for all heavy particles ($0 \leq R < \frac{2}{3}$) and light particles ($\frac{2}{3} < R \leq 1$) but is most strongly exhibited in the extreme aerosol ($R = 0$) and bubble ($R = 1$) cases. Additionally, recall that as the periodic frequency ω increases, the FTLE fields become more complicated. The coherent structures associated with these FTLE fields are therefore complex. For clarity, we only explore the behavior of the extreme density ratio values within a slow sloshing quasi-geostrophic model.

Inertial particles exhibit the same preferential aggregation behavior in the quasi-geostrophic flow as they do in the simpler double-gyre flow. Figures 16 and 17 highlight the clustering of

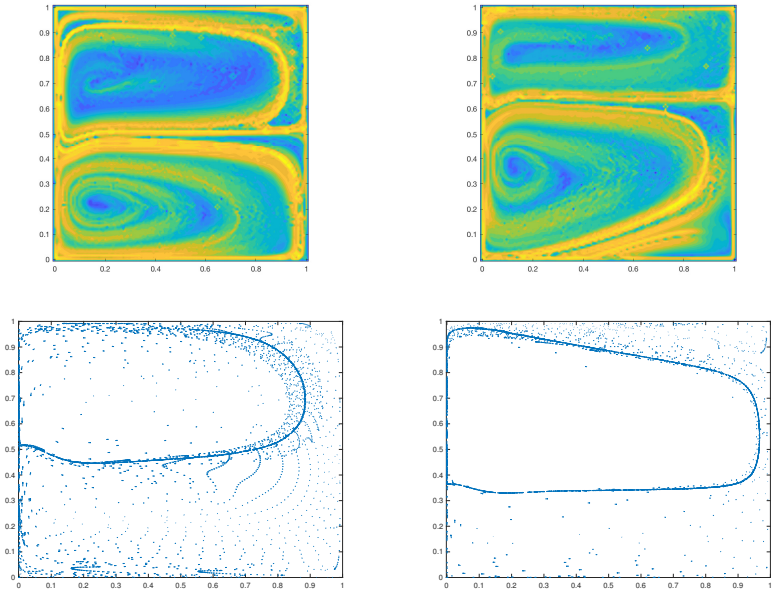

Figure 16: Preferential aggregation of heavy inertial particles in the quasi-geostrophic flow with slow periodic sloshing $\omega = 1$ at times $t = 1.25$ and $t = 2.5$. This clustering behavior corresponds to the second and third fluid FTLE fields in Fig. 7 which are shown again here for ease of comparison.

aerosols and bubbles respectively at $t = 1.25$ and $t = 2.5$. Comparison of these inertial particle clusters with the quasi-geostrophic fluid FTLE fields shown in Fig. 7 show great agreement with the conclusions drawn from the double-gyre model in each analogous case. Figure 16 shows heavy particles advecting along the most defined FTLE ridge. Interestingly, despite the presence of additional structures, the thin ridge with the highest FTLE values seems to dominate the inertial particle behavior.

In Fig. 17, we see light particles exhibit some interesting behavior. As expected, we see particles aggregating in the center of the two vortices. However, there is also an apparent clustering of the bubbles along the strong FTLE ridge. This is unexpected behavior for light inertial particles, as they have been shown to repel from LCS in the double-gyre model. Recall, however, that the quasi-geostrophic model is subject to a thin-layer, western boundary effect. We have shown that for neutrally buoyant particles, this western boundary effect causes some funneling behavior along the FTLE ridge. We suspect that in the case of bubbles, this western boundary effect influences some particles to be funneled toward the high FTLE ridge, while othe particlesr remain trapped in the gyres, and exhibit their expected clustering behavior. Further analysis is needed to corroborate this suspicion.

6 Summary and Remarks

We have presented a theoretical and numerical approach for understanding the transport of inertial particles in geophysical flows. Specifically, we highlight the finite-time Lyaponuv exponents as a

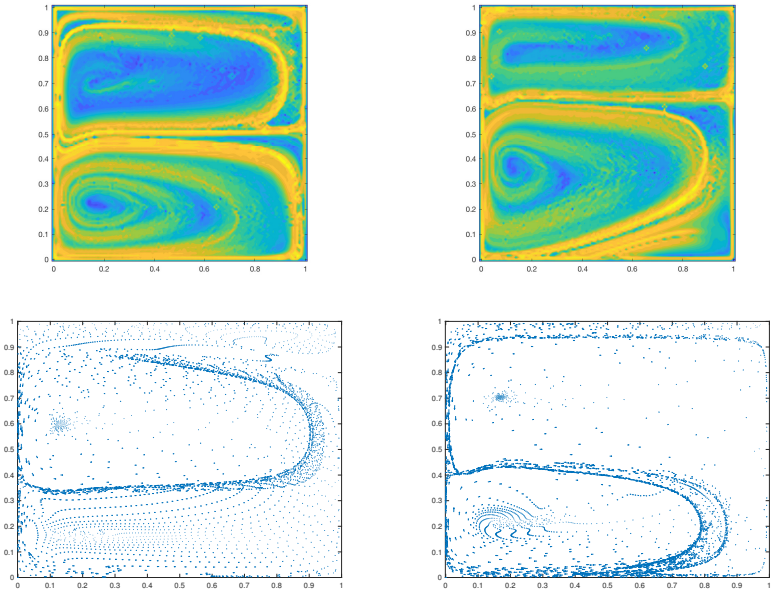

Figure 17: Preferential aggregation of light inertial particles in the quasi-geostrophic flow with slow periodic sloshing $\omega = 1$ at times $t = 1.25$ and $t = 2.5$. This clustering behavior corresponds to the second and third fluid FTLE fields in Fig. 7 which are shown again here for ease of comparison.

tool for distinguishing Lagrangian coherent structures which are crucial to understanding how fluid and inertial particles traverse through the ocean. The results in this work have implications to a variety of applications, but in particular, they are extremely useful in determining energy and time optimal path trajectories for autonomous underwater vehicles.

We numerically computed the FTLE fields for two fluid models, the double-gyre ODE model, and the more realistic quasi-geostrophic PDE model. We show that high FTLE ridges, corresponding to fluid LCS, do influence the transport of inertial particles. In the standard case of each model, heavy particles $R > \frac{2}{3}$ attract along thin, high FTLE valued bands. As $R \to 1$ this preferential aggregation behavior is stronger. Heavier aerosols will advect more quickly to the coherent structures and their clusters are more well-defined. As $R \to \frac{2}{3}$ from either side, the inertial particles start to behave like passive tracer particles. They exhibit little to no clustering behavior and in general, trace out the trajectories of the underlying fluid flow. As $R \to 0$, light particles tend to be repelled by high FTLE regions. They exhibit clustering behavior in the center of the gyres where FTLE values are relatively low. The lightest particles, with $R = 1$, exhibit the strongest clustering behavior, creating tight clusters in the center of the gyres. We can conclude that LCS act as attracting regions for aerosols and repelling regions for bubbles and that these behaviors are strengthened as the difference between the density of the particle and the carrier fluid is increased.

We have also shown the effects of Stokes number on inertial particle aggregation matches our intuition. Since St is a characteristic relaxation time of the particle to the fluid flow, we expect that particles will take longer to relax to the flow in high Stokes regimes and will follow the flow closely in very low Stokes regimes. Due to the form of Eq. 2, we can only achieve sufficient accuracy for $St \geq 0.01$. For Stokes numbers smaller than this, we introduce numerical instabilities.

Nevertheless, our results for varied Stokes number flows support our intuition that Stokes number affects the speed at which the particles exhibit their preferential aggregation behavior. In high Stokes number flows, bubbles take longer to cluster in the gyre centers and aerosols do not move as quickly to thin structures. In low Stokes number regimes, the particles exhibit their preferential aggregation behavior more quickly.

We also qualitatively show the effects of Coriolis force on inertial particle dynamics. In the double-gyre model, the presence of Coriolis force strengthens the attractors at the center of each gyre. This attraction works in the favor of bubbles, as they prefer to cluster in the gyre center. Accounting for Coriolis force, we see bubbles exhibit their clustering behavior quicker and form tighter clusters. While the Coriolis force acts as a catalyst for the clustering of light particles, it hinders the clustering of heavy particles. Aerosols want to cluster away from either gyre center and onto central high FTLE bands. With the Coriolis force influencing inertial particles towards the center of the gyres, aerosols have to work against this attraction to aggregate along LCS. They are still successful in aggregating along high FTLE bands. However, the Coriolis force slows down this transport behavior.

In the quasi-geostrophic model, we see even more interesting transport behavior. The thin western boundary layer adds an additional aspect to inertial particle transport. The boundary layer causes particles to be funneled into the mixing region of the stacked double-gyres which has varied effects on inertial particle aggregation. Neutrally buoyant particles, which should exhibit no clustering behavior, show aggregation along the thin bands like aerosols do. Bubbles, which usually cluster in the center of the gyres only, show clustering in both the center of the gyres and the same thin bands. Aerosol aggregation behavior stays as expected, but is even stronger. These changes in aggregation behavior show that the thin western boundary layer influences more mixing of inertial particles by funneling particles through the thin bands between gyres, a region characterized by high stretching and mixing.

It is clear from these numerical results that fluid LCS do, in fact, influence the transport of inertial particles. LCS act as attracting regions for heavy particles and repelling regions for light particles. For the models we considered, the Coriolis force hinders the attraction of LCS but strengthens their repulsion. Additionally, other influences such as Stokes number and western boundary effects, can speed up or slow down aggregation behavior and promote new behaviors all together. Continued study of the relationship between LCS and inertial particle transport is important to use sensing AUVs in energy and time optimal ways. These AUVs can numerically compute LCS and use this aggregation information to make informed decisions on their paths. With this knowledge, AUVs can aid in making more accurate weather predictions, performing faster discovery of oil spill sources, and improving the tracking of contaminants in the ocean. Our work allows AUVs to be more successful as they perform sensing task that are important to the global community.

7 Bibliography

References

[1] R. Pierrehumbert and H.Yang, "Global chaotic mixing on isentropic surfaces," Journal of Atmospheric Sciences, vol. 50, no. 15, pp. 2462–80, 1992.

[2] G. Haller, "Distinguished material surfaces and coherent structures in three-dimensional fluid flows," Physica D, vol. 149, pp. 248–77, 2001.

[3] T. Peacock and G. Haller, "Lagrangian coherent structures: The hidden skeleton of fluid flows," Physics Today, vol. 66, no. 2, p. 41, 2013.

[4] R. A. Shaw, W. Reade, L. Collins, and J. Verlinde, "Preferential concentration of cloud droplets by turbulence: Effects on the early evolution of cumulus cloud droplet spectra," Journal of the Atmospheric Sciences, vol. 55, pp. 1965–1976, 06 1998.

[5] T. Sapsis and G. Haller, "Inertial particle dynamics in a hurricane," Journal of the Atmospheric Sciences, vol. 66, no. 8, pp. 2481–2492, 2009.

[6] F. Paparella, A. Babiano, C. Basdevant, A. Provenzale, and P. Tanga, "A lagrangian study of the antarctic polar vortex," Journal of Geophysical Research: Atmospheres, vol. 102, no. D6, pp. 6765–6773.

[7] N. Raju and E. Meiburg, "Dynamics of small, spherical particles in vortical and stagnation point flow fields," Physics of Fluids, vol. 9, no. 2, pp. 299–314, 1997.

[8] I. J. Benczik, G. Károlyi, I. Scheuring, and T. Tél, "Coexistence of inertial competitors in chaotic flows," Chaos: An Interdisciplinary Journal of Nonlinear Science, vol. 16, no. 4, p. 043110, 2006.

[9] I. Mezic, S. Loire, V. Fonoberov, and P. Hogan, "A new mixing diagnostic and gulf oil spill movement," Science, vol. 330, pp. 486–9, 10 2010.

[10] M. J. O. F.J. Beron-Vera and G. Goni, "Oceanic mesoscale eddies as revealed by lagrangian coherent oceanic mesoscale eddies as revealed by lagrangian coherent structures," Geophysical Research Letters, vol. 35, 2008.

[11] J. Peng and J. O. Dabiri, "Transport of inertial particles by lagrangian coherent structures: Application to predator-prey interaction in jellyfish feeding," Journal of Fluid Mechanics, vol. 623, 03 2009.

[12] E. R. Abraham, C. S. Law, P. W. Boyd, S. J. Lavender, M. T. Maldonado, and A. R. Bowie, "Importance of stirring in the development of an iron-fertilized phytoplankton bloom," Nature, vol. 407, pp. 727 EP –, 10 2000.

[13] E. F. M. Michini, M.A. Hsieh and I. Schwartz, "Robotic tracking of coherent structures in flows,," IEEE Transactions on Robotics, vol. 30, no. 3, pp. 593–603, 2014.

[14] "www.lpi.usra.edu/publications/slidesets/oceans/oceanviews/slide_03.html."

[15] "https://commons.wikimedia.org/wiki/file:deepwater_horizon_oil_spill_-_may_24,_2010_-_with_locator.jpg."

[16] "news.algaeworld.org/2017/10/orbitalviewofalgalbloomsinlakeerie/."

[17] "scripps.ucsd.edu/news/revisitingseaplex."

[18] M. R. Maxey and J. J. Riley, "Equations of motion for a small rigid sphere in nonuniform flow," The Physics of Fluids, vol. 26, p. 883, 1983.

[19] A. Babiano, "Dynamics of a small neutrally buoyant sphere in a fluid and targeting in hamiltonian systems," Physical Review Letters, vol. 84, no. 25, pp. 5764–5767, 2000.

[20] T. Tél, A. Moura, C. Grebogi, and G. Károlyi, "Chemical and biological activity in open flows: A dynamical system approach," Physics Reports, vol. 4135370, 07 2005.

[21] E. E. Michaelides, "Review—the transient equation of motion for particles, bubbles, and droplets," Journal of Fluids Engineering, vol. 119, pp. 233–247, 06 1997.

[22] A. Daitche and T. Tél, "Memory effects in chaotic advection of inertial particles," New Journal of Physics, vol. 16, p. 073008, July 2014.

[23] M. Sudharsan, S. L. Brunton, and J. J. Riley, "Lagrangian coherent structures and inertial particle dynamics," Physical Review E, vol. 93, no. 3, 2016.

[24] G. Haller and G. Yuan, "Lagrangian coherent structures and mixing in two-dimensional turbulence," Phys. D, vol. 147, pp. 352–370, Dec. 2000.

[25] G. Haller, "Lagrangian coherent structures," Annual Review of Fluid Mechanics, vol. 47, pp. 137–62, 2015.

[26] G. Haller, "Lagrangian coherent structures from approximate velocity data," Physics of Fluids, vol. 14, no. 6, pp. 1851–1861, 2002.

[27] S. C. Shadden, Transport and Mixing in Laminar Flows: From Microfluidics to Ocean Currents. Wiley-VCH Verlag GmbH and Co., 2012.

[28] M. Farazmand and G. Haller, "The maxey-riley equation: Existence, uniqueness and regularity of solutions," Nonlinear Analysis: Real World Applications, 10 2013.

[29] S. C. Shadden, F. Lekien, and J. E. Marsden, "Definition and properties of lagrangian coherent structures from finite-time lyapunov exponents in two-dimensional aperiodic flows," Physica D, vol. 212, pp. 271–304, 2005.

[30] A. Basset, "On the motion of a sphere in a viscous liquid," Philosophical Transactions of the Royal Society of London, vol. 179, pp. 43–63, 1888.

[31] W. H. Munk, "On the wind-driven ocean circulation," Journal of Meterology, vol. 7, no. 2, 1950.

[32] E. Forgoston, L. Billings, P. Yecko, and I. B. Schwartz, "Set-based corral control in stochastic dynamical systems: Making almost invariant sets more invariant," Chaos, 01 2011.

[33] H. Stommel, "The westward intensification of wind-driven ocean currents," Transactions, American Geophysical Union, vol. 29, no. 2, 1948.

[34] J. Pedlosky, Geophysical Fluid Dynamics. Springer-Verlag New York, 2 ed., 1987.

[35] A. Provenzale, "Transport by coherent barotropic vortices," Annual Review of Fluid Mechanics, vol. 31, no. 1, pp. 55–93, 1999.